OCEANOGRAPHY

Regulation of calcification site pH is a polyphyletic but not always governing response to ocean acidification

Yi-Wei Liu[1,2]*, Jill N. Sutton[1], Justin B. Ries[3], Robert A. Eagle[1,4,5]*

The response of marine-calcifying organisms to ocean acidification (OA) is highly variable, although the mechanisms behind this variability are not well understood. Here, we use the boron isotopic composition (δ^{11}B) of biogenic calcium carbonate to investigate the extent to which organisms' ability to regulate pH at their site of calcification (pH_{CF}) determines their calcification responses to OA. We report comparative δ^{11}B analyses of 10 species with divergent calcification responses (positive, parabolic, threshold, and negative) to OA. Although the pH_{CF} is closely coupled to calcification responses only in 3 of the 10 species, all 10 species elevate pH_{CF} above pH_{sw} under elevated pCO_2. This result suggests that these species may expend additional energy regulating pH_{CF} under future OA. This strategy of elevating pH_{CF} above pH_{sw} appears to be a polyphyletic, if not universal, response to OA among marine calcifiers—although not always the principal factor governing a species' response to OA.

INTRODUCTION

Uptake of CO_2 by the oceans reduces calcium carbonate saturation state $\left(\Omega = \frac{[Ca^{2+}][CO_3^{2-}]}{K_{sp}} \right)$ of seawater. Some areas of the surface ocean have already become undersaturated, which promotes $CaCO_3$ dissolution, with predictions that these areas will substantially expand throughout the century (1–3). A reduction in Ω is expected to make it more difficult for $CaCO_3$-mineralizing organisms to produce their shells and skeletons, with deleterious impacts on the fitness of those organisms (1–6). Laboratory-based studies and field observations have shown a diversity in the response of marine calcifying organisms to CO_2-manipulated saturation state (5, 7, 8). Some species exhibit a more predictable negative net calcification response to CO_2-induced reductions in Ω, while others exhibit relative resilience and even positive net calcification responses (5, 7, 8).

One of the first experimental studies to characterize the full diversity of responses to CO_2-induced ocean acidification (OA), including positive calcification responses, was presented by Ries et al. (5). The underlying reasons for these diverse responses are potentially complex, given the significant biological differences among the taxa studied. However, Ries (9) proposed a relatively parsimonious physicochemical model whereby these diverse net calcification responses could potentially be explained by differences in species' ability to regulate pH and carbonate ion concentration ($[CO_3^{2-}]$) of the fluid from which they form $CaCO_3$ through active removal of protons. This model proposes that an organism with a high proton-pumping capacity may be more resilient—in some cases even faster calcifying—under OA conditions by maintaining (or increasing) $[CO_3^{2-}]$ at the site of calcification under elevated atmospheric pCO_2.

Species with lower proton-pumping capacity would exhibit relatively negative responses to OA (parabolic to threshold negative to linearly negative) due to decreasing $[CO_3^{2-}]$ at the site of calcification with increasing atmospheric pCO_2. Other views of biomineralization, for example, highlighted in studies of echinoderms, mollusks, and scleractinian corals (10–13), hold that $CaCO_3$ biomineral formation within many species of calcifiers is not only influenced by pH and $[CO_3^{2-}]$ at the site of calcification but may instead commence intracellularly or in tightly regulated extracellular compartments and be controlled by organic molecules that, for example, induce crystal nucleation, guide crystal growth, and/or modulate the transformation of amorphous calcium carbonate (ACC) precursors into crystalline aragonite or calcite. It should be noted, however, that the two models are not necessarily incompatible, as calcification site chemistry and organic molecules may both influence the formation and distribution of $CaCO_3$ minerals in the shell-building process.

Here, we revisit the Ries et al. (5) study by using the boron isotope composition of biogenic $CaCO_3$ material produced under a range of pCO_2 conditions to investigate the extent to which pH control at the site of calcification is coupled to net calcification responses to CO_2-induced OA within a divergent suite of marine-calcifying organisms. We analyzed the boron isotope composition of the shells/skeletons of 10 species of marine calcifiers, including mollusks, crustaceans, echinoids, scleractinian corals, serpulid worms, and coralline algae, which were previously cultured at four pCO_2 conditions spanning ca. 400 to 2850 parts per million (5). This suite of species collectively exhibits the full range of calcification response patterns to CO_2-induced OA observed in the original study (5), as well as in most subsequent studies to date (6) (Fig. 1, fig. S1, and table S1).

RESULTS AND DISCUSSION

We found that shell/skeletal δ^{11}B composition varied widely among the investigated species (Fig. 1 and table S1). In most cases, skeletal/shell δ^{11}B deviates from the theoretical relationship between seawater borate δ^{11}B and pH_{sw}, consistent with prior studies that have inferred biological control over pH_{CF} from offsets between skeletal/shell δ^{11}B and external seawater borate δ^{11}B for many types of marine calcifiers [e.g., (14–20)].

[1]Université de Brest, UBO, CNRS, IRD, Ifremer, Institut Universitaire Européen de la Mer, LEMAR, Rue Dumont d'Urville, 29280 Plouzané, France. [2]Institute of Earth Sciences, Academia Sinica, 128, Sec. 2, Academia Road, Nangang, Taipei 11529, Taiwan. [3]Department of Marine and Environmental Sciences, Marine Science Center, Northeastern University, 430 Nahant Rd., Nahant, MA 01908, USA. [4]Institute of the Environment and Sustainability, University of California–Los Angeles, La Kretz Hall, 619 Charles E. Young Dr. E #300, Los Angeles, CA 90095, USA. [5]Atmospheric and Oceanic Sciences Department, University of California–Los Angeles, Math Sciences Building, 520 Portola Plaza, Los Angeles, CA 90095, USA.
*Corresponding author. Email: liuyiwei@earth.sinica.edu.tw (Y.-W.L.); robeagle@g.ucla.edu (R.A.E.)
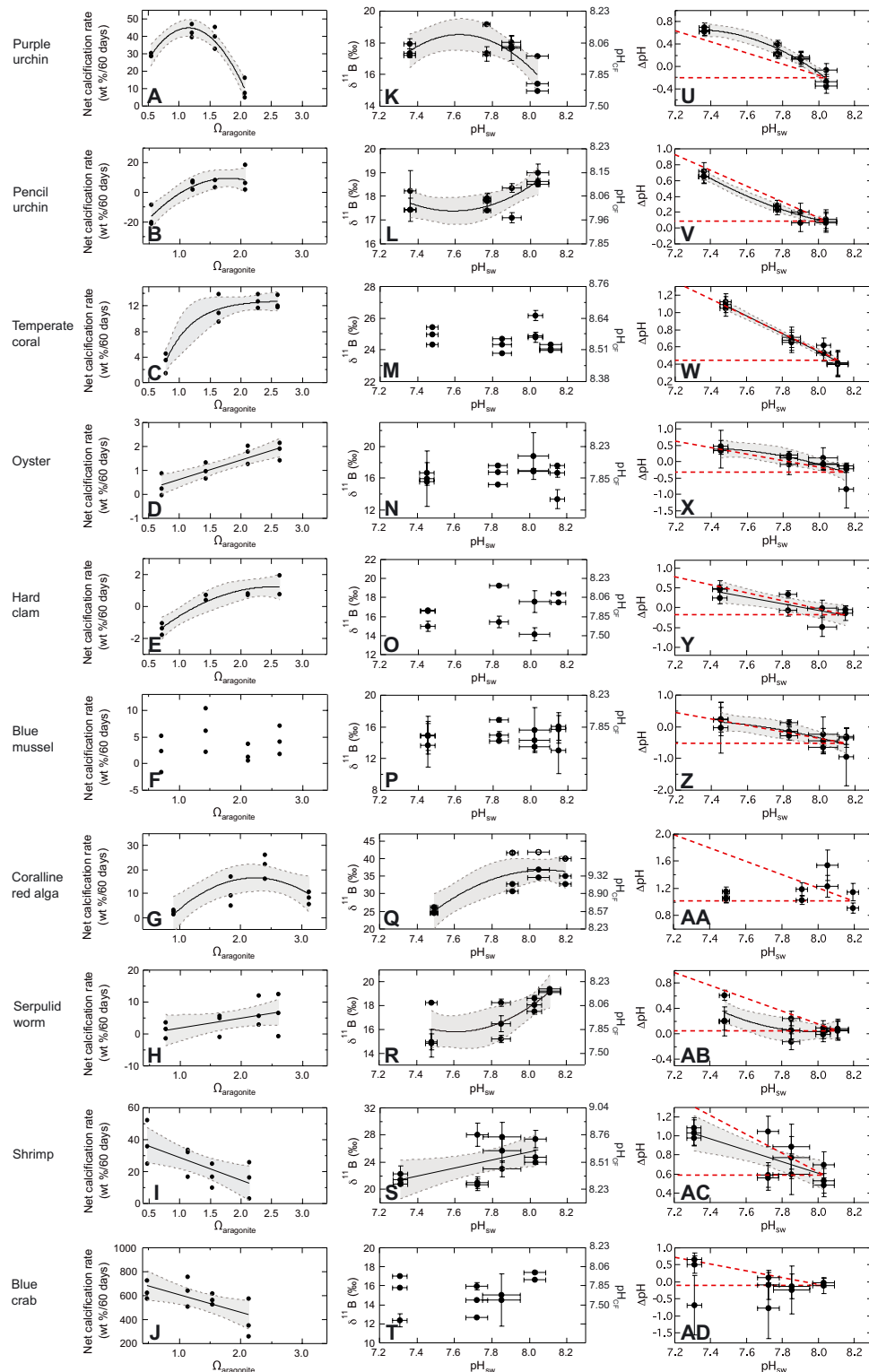
Fig. 1. Comparison of net calcification rate, $\delta^{11}B$, pH_{CF}, and ΔpH ($pH_{CF} - pH_{sw}$) responses to CO$_2$-induced OA for the 10 investigated species of marine calcifiers. (**A**) to (**J**) net calcification responses of the 10 species to OA. (**K**) to (**T**) $\delta^{11}B$ values of the 10 species and the boron-inferred pH_{CF} values versus pH_{sw}. (**U**) to (**AD**) pH offsets of the 10 species versus pH_{sw}; the pH control envelope, bounded by red dashed lines (see also Fig. 2) is superimposed over each plot. The $\delta^{11}B$ compositions of the 10 species ranged from 11 to 41‰, with coralline red algae exhibiting the highest $\delta^{11}B$, followed by shrimp, temperate corals, urchins, serpulid worms, mollusks, and crabs. Values of pH_{CF} estimated from measured $\delta^{11}B$ are plotted using the right axes of (K) through (T). In panels (U) to (AD), ΔpH-pH_{sw} trends below, within, and above the envelope indicate weak, moderate, and strong control over pH_{CF}. Significant trends ($P > 0.05$) with 95% confidence levels are plotted as solid and dashed curve lines, respectively (see tables S1 to S3 for regression statistics). wt %, weight %.
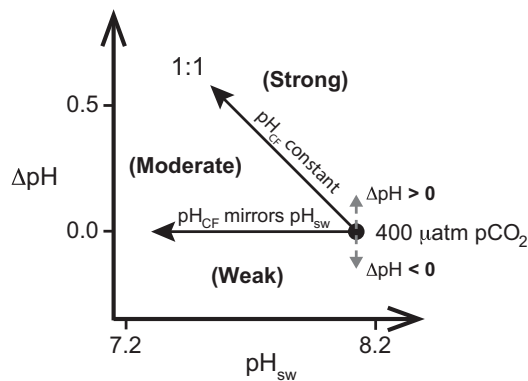
Fig. 2. Schematic diagram of the "pH control envelope" to aid interpretation of ΔpH trends as a function of pH$_{sw}$. The upper boundary of the pH control envelope is defined by a 1:1 relationship between ΔpH and pH$_{sw}$, such that pH$_{CF}$ remains constant regardless of pH$_{sw}$. The lower boundary is defined by the scenario in which ΔpH remains fixed regardless of pH$_{sw}$, such that changes in pH$_{CF}$ track changes in pH$_{sw}$. The envelope therefore describes three categories of pH$_{CF}$ control: weak control at or below the lower bound of the envelope, moderate control within the envelope, and strong control at or above the upper bound of the envelope. The apex of the envelope is translated up or down relative to ΔpH = 0 if pH$_{CF}$ is respectively greater or less than pH$_{sw}$ under control pCO$_2$ conditions.

Although plotting δ^{11}B versus CO$_2$ is the most parsimonious visualization of the data, we plot pH$_{CF}$ (calculated from shell/skeletal δ^{11}B; see Materials and Methods) for each species across the four pCO$_2$ treatments from the δ^{11}B composition of the species' shells or skeletons (see Materials and Methods) and show these alongside δ^{11}B values in Fig. 1 (K to T). This methodology requires several key assumptions, including that the studied organisms precipitate their shells or skeletons from a discrete medium that is at least partially isolated from seawater (i.e., the calcifying fluid), that both the δ^{11}B composition of total boron and the acid dissociation constant for boron (pK$_B$) in the calcifying fluid and the surrounding seawater are equivalent, that borate is the primary form of boron incorporated into the shells and skeletons of the studied organisms, and that the boron isotope fractionation factor used in the present study [Klochko et al. (21)] is accurate. Each of these assumptions has been thoroughly explored for a number of species in previous publications (16, 19) and is reviewed in the Supplementary Materials.

To our knowledge, these are the first reported measurements of δ^{11}B on the carbonate component of crustacean carapace, as well as the first reported estimates of pH$_{CF}$ for crustacea. The complex nature of crustacean carapaces—which contain both chitin and carbonate components distributed within organic matrices—and uncertainty over how this material responds during the dissolution and purification steps of preparing the sample for δ^{11}B analysis may introduce additional uncertainties in the quantitative interpretation of the resulting δ^{11}B data. Furthermore, unlike many of the species examined here, the authors are not aware that any independent measurements of pH$_{CF}$ in crustacea have been obtained using different techniques, which precludes cross-validation of the pH$_{CF}$ values estimated here for crustacea.

The δ^{11}B data exhibit parabolic, neutral, threshold-negative, and negative trends with decreasing pH$_{sw}$ (Fig. 1) with the coralline red alga (see the Supplementary Materials for discussion of elevated δ^{11}B values), purple urchin, and blue mussel exhibiting δ^{11}B-pH$_{sw}$ patterns that most closely mirror their net calcification response

patterns (Fig. 1). These results indicate that calcifying species exhibit a wide range of capacities for modifying pH$_{CF}$ in response to OA (table S1) and that a species' specific capacity for pH$_{CF}$ regulation does not necessarily dictate its unique calcification response to OA. Notably, however, we found that all 10 species of calcifiers elevated pH$_{CF}$ relative to pH$_{sw}$ in at least one of the acidified treatments, with 9 of 10 species increasing the magnitude that pH$_{CF}$ is elevated relative to pH$_{sw}$ (ΔpH) with increasing pCO$_2$. The coralline red algae, temperate corals, shrimp, and urchins elevated pH$_{CF}$ above pH$_{sw}$ under all pH$_{sw}$ conditions, while the oyster, hard clam, blue mussel, blue crab, and serpulid worm species elevated pH$_{CF}$ relative to pH$_{sw}$ only under some acidified conditions. Of this latter group, the serpulid worm and blue crab maintained a pH$_{CF}$ similar to pH$_{sw}$ under control conditions, while the pH$_{CF}$ of the three mollusk species—the oyster, hard clam, and blue mussel—was maintained at a lower pH than pH$_{sw}$ under control conditions. Notably, the mollusks, blue crabs, and temperate corals also maintained a relatively constant pH$_{CF}$ across pH$_{sw}$ conditions, with pH$_{CF}$ averaging ca. 7.8 for the mollusks, 8.0 for the blue crabs, and 8.5 for the temperate corals. The boron-inferred pH$_{CF}$ values in this study are generally within the range of previous δ^{11}B-based, pH microelectrode–based, and pH-sensitive dye–based estimates of pH$_{CF}$ for many types of marine calcifiers, including corals (22, 23) and mollusks (24).

We can also evaluate the extent to which the different species modify pH$_{CF}$ relative to pH$_{sw}$ (ΔpH = pH$_{CF}$ − pH$_{sw}$) under different OA scenarios by superimposing a schematic "pH control envelope" (Fig. 2) on each species' ΔpH-pH$_{sw}$ plot (Fig. 1). The upper boundary of this envelope is defined by a 1:1 relationship between ΔpH and pH$_{sw}$, such that species falling on this line maintain constant pH$_{CF}$ as external pH$_{sw}$ declines. The lower boundary of the pH control envelope is defined by the scenario in which organisms maintain a fixed ΔpH, independent of pH$_{sw}$, such that changes in pH$_{CF}$ directly track changes in pH$_{sw}$. The envelope therefore describes three categories of pH$_{CF}$ control as follows: weak control at or below the lower boundary of the envelope, moderate control toward the center of the envelope, and strong control at or above the upper boundary (Fig. 2).

Consideration of the ΔpH versus pH$_{sw}$ plots (Fig. 1) in the framework of the pH control envelope (Fig. 2 and table S3) permits additional inferences about the role of pH$_{CF}$ control in driving species-level differences in calcification response to OA. For instance, ΔpH for the purple urchin varies parabolically with pH$_{sw}$, with a trend falling completely above the upper edge (i.e., 1:1 line) of the pH control envelope (Fig. 1). This finding indicates that the purple urchin has relatively strong control over pH$_{CF}$ to the extent that it can raise pH$_{CF}$ when pCO$_2$ increases, thereby converting some of the dissolved inorganic carbon (DIC) at the site of calcification into additional CO$_3^{2-}$ for calcification—although the parabolic response of δ^{11}B to pH$_{sw}$ indicates that this capacity is dampened for the purple urchin under extreme pCO$_2$. This parabolic trend in the purple urchin's δ^{11}B-pH$_{sw}$ relationship is notably similar to its parabolic calcification responses to elevated pCO$_2$ (Fig. 2), suggesting that purple urchin's calcification response to OA is largely dictated by its degree of control over pH$_{CF}$. In contrast to the purple urchin, the pencil urchin exhibits δ^{11}B and, by extension, pH$_{CF}$ that decreases asymptotically with pH$_{sw}$—suggesting that this species maintains a minimum pH$_{CF}$ regardless of pH$_{sw}$. The observation that the ΔpH-pH$_{sw}$ trend (Fig. 1) for the pencil urchin falls in the central-upper region of the pH control envelope (moderate-strong pH$_{CF}$ control) is consistent with the pencil

Table 1. Summary of the growth, boron isotope/boron–derived pH_{CF}, and ΔpH patterns as a function of aragonite saturation state or seawater pH and the inferred pH_{CF} regulation ability of the investigated organisms.

Organism	Net calcification response to pCO_2*	$\delta^{11}B(pH_{CF})$ response to pCO_2†	ΔpH response to pH_{sw}‡	Ability to control pH_{CF} in response to pCO_2 increase§
Purple urchin	Parabolic	Parabolic	Positive	Strong
Pencil urchin	Threshold negative	Nonlinear negative	Nonlinear positive	Moderate/Strong
Temperate coral	Threshold negative	Neutral	Positive	Moderate/Strong
Oyster	Negative	Neutral	Nonlinear positive	Moderate/Strong
Hard clam	Threshold negative	Neutral	Positive	Moderate/Strong
Blue mussel	Neutral	Neutral	Nonlinear positive	Moderate/Strong
Coralline red alga	Parabolic	Parabolic	Neutral	Moderate
Serpulid worm	Negative	Nonlinear negative	Nonlinear positive	Moderate
Shrimp	Positive	Negative	Positive	Moderate
Blue crab	Positive	Neutral	Neutral	Weak

*The net calcification response to variable pCO_2 conditions as reported in Ries *et al.*, (*5*). † and ‡Describes direction and shape of the best-fit regression of the $\delta^{11}B$ and ΔpH as a function of seawater pH, respectively, via the least squares method. Detailed analysis is available in tables S2 and S3. The patterns are also shown in Fig. 1. §A species' ability to control pH_{CF} in response to pCO_2 increase is classified based on ΔpH versus pH_{sw} trends relative to the theoretical pH control envelope (Fig. 2), not to the absolute offset of pH_{CF} relative to pH_{sw} under a single treatment.

urchin's semiresilient threshold-negative calcification response to OA (Fig. 1). The difference in $\delta^{11}B$ calcification patterns (Fig. 1) between the two species may arise from the different habitats of the two species, with the temperate purple urchin experiencing lower and more variable pH conditions than the pencil urchin due to the elevated solubility of CO_2 and increased upwelling of the purple urchin's colder, higher latitude shelf environments versus the tropical carbonate bank environment of the pencil urchin, potentially rendering the purple urchin better adapted for calcification under challenging environmental conditions.

Analysis of $\delta^{11}B$ within the temperate coral suggests that this species maintains an elevated but relatively constant pH_{CF} (ca. 8.5 pH_{CF}) across pCO_2 treatments (Fig. 1). The temperate coral's ΔpH-pH_{sw} trend falls directly on the 1:1 line of the pH control envelope (Figs. 1 and 2), indicating that this species exhibits moderate-to-strong control over pH_{CF} when exposed to OA. Likewise, net calcification rates were also relatively constant across pCO_2 treatments, except in the highest pCO_2 treatment, where they declined precipitously, which can at least be partly explained by rapid dissolution of exposed skeleton [previously documented at rates up to ca. 7 weight %/60 days in aragonite-undersaturated seawater (*25*)], rather than by the unfavorable conditions at the site of calcification.

Analyses of $\delta^{11}B$ within shells of the investigated mollusk species, including the oyster, hard clam, and blue mussel, indicate that they, like the temperate coral, maintain a relatively constant pH_{CF} (average pH_{CF} ~7.8) across pCO_2 treatments—but at a level substantially lower than the pH_{CF} maintained by the other species investigated. However, unlike all of the other species, the mollusks maintain pH_{CF} below pH_{sw} under the control pCO_2 treatment, but above the pH_{sw} in the elevated pCO_2 treatments. The observation that ΔpH-pH_{sw} trends for the mollusks are close to the 1:1 line of the pH control envelope (Fig. 1) suggests that the mollusks exert moderate-to-strong control over pH of their calcifying fluid—their so-called extrapallial fluid. However, the blue mussel is the only mollusk in our study that exhibits a calcification response to elevated pCO_2 (neutral) consistent with strong control over pH_{CF}. The calcification responses of the hard

clam and oyster are more negative and, thus, decoupled from their apparently strong control over pH_{CF}. This apparent decoupling of pH_{CF} control and calcification responses within mollusks may reflect the apparently important roles that other physiological factors, such as ACC precursor mineral phases, organic molecules, and proteinaceous mineral templates, play in their biomineralization (*10*).

Analysis of $\delta^{11}B$ within the coralline red alga indicates that the pH_{CF} of this species varies parabolically with pCO_2 and exhibits a substantial drop in pH_{CF} under the highest pCO_2 treatment. The ΔpH for the coralline red alga also varies with pH_{sw}, with the trend line falling above the upper boundary of the pH control envelope (Fig. 1) under higher pH_{sw} conditions and near the lower boundary under lower pH_{sw} conditions. This indicates an initially strong control over pH_{CF} of the coralline red alga, with this control diminishing under higher pCO_2 conditions.

Analysis of $\delta^{11}B$ within the calcareous tube of the serpulid worm (Fig. 1) indicates that pH_{CF} decreases asymptotically with pH_{sw}, suggesting that this species maintains a minimum pH_{CF} regardless of pH_{sw}. The ΔpH trend for the serpulid worm falls in the lower portion of the pH control envelope (moderate pH_{CF} control), which is consistent with its linearly negative calcification response to increasing pCO_2 (Figs. 1 and 2).

Analyses of $\delta^{11}B$ within the crustaceans, including the blue crab and shrimp species, indicate that they too maintain elevated pH_{CF} relative to pH_{sw} at the higher pCO_2 treatments. In both species, pH_{CF} declines with decreasing pH_{sw}. The shrimp, however, maintains a higher pH_{CF} than that of the blue crab. The observation that ΔpH-pH_{sw} trends fall toward the center of the pH control envelope (Fig. 1) for the shrimp and toward the bottom for the crab suggests that these crustaceans exert only weak-to-moderate control over their pH_{CF}, which is inconsistent with their unique, strongly positive net calcification responses to elevated pCO_2. This apparent discrepancy may arise from the crustacean molting style of biomineralization, which requires them to mineralize an entirely new shell in a matter of hours to minimize exposure to predation during their soft-bodied phase.

It is logical that this molting style of biomineralization would select for strong biological controls on calcification beyond, or in addition to, pH_{CF} control to shorten their vulnerable soft-shelled stage, which may ultimately render crustacea particularly resilient to OA.

Values of ΔpH indicate that all of the investigated species elevated pH at their site of calcification relative to pH of their surrounding seawater under at least one of the elevated pCO_2 treatments. However, the considerable interspecies variation in ΔpH patterns across experimental treatments indicates that the complex physiological controls that govern a species' response to OA may be as diverse as the range of species examined. Nevertheless, the overall results of the present study are consistent with the assertion that the more control that a species exerts over its pH_{CF}, the greater its resilience to OA, although some species, such as the crustacea, demonstrate relatively strong resilience to OA despite exhibiting only weak-to-moderate control over pH_{CF} (Table 1).

A species' ability to control pH_{CF} will be influenced by multiple factors, including the residence time of the calcifying medium, proton transport and diffusion, formation and dissolution of shell/skeleton, input of DIC via respiration, DIC transport and diffusion, DIC respeciation (including via the activity of enzymes like carbonic anhydrase), and, in the case of photosynthetic organisms, the photosynthetic drawdown of DIC. The rates of these processes may change under acidified conditions, either as a passive response to acidification (e.g., increased shell dissolution) or as an adaptive response by the organism (e.g., increased proton pumping under acidified conditions). Rates of photosynthesis within marine algae have also been shown to increase under elevated pCO_2, up to the point that CO_2 is no longer limiting for photosynthesis, and rates of DIC drawdown and proton release via calcification typically change under acidified conditions, both potentially affecting pH_{CF}. For example, diel variations in extracellular pH of the calicoblastic tissue of scleractinian corals have been attributed to daily cycles of respiration and photosynthesis (22), and observations of pH up to 9 within the diffusive boundary layer of algal turfs have been ascribed to the algae's photosynthetic drawdown of aqueous CO_2 (26). The balance of these diverse processes influencing carbonate chemistry at the site of calcification may explain the range of pH_{CF} versus pH_{sw} relationships observed in the present experiment.

CONCLUSIONS

Boron isotope analysis of the shells and skeletons of 10 divergent marine-calcifying species cultured under various pCO_2 conditions reveals considerable interspecific differences in the regulation of pH_{CF} in response to OA. Although pH_{CF}-pH_{sw} trends for a few of the species, including the purple urchin, coralline alga, and blue mussel, mirror net calcification responses to OA, these trends are decoupled in the majority of the species investigated, including the temperate coral, pencil urchin, hard clam, shrimp, blue crab, serpulid worm, and oyster. Despite this apparent disparity in the role that pH_{CF} control plays in marine calcifiers' specific calcification response to OA, we observed that all 10 species adopted the chemically beneficial strategy of maintaining pH_{CF} above pH_{sw} ($\Delta pH > 0$) under elevated pCO_2 conditions, indicating that the elevation of pH_{CF} relative to pH_{sw} is a polyphyletic, if not universal, response among marine calcifiers to OA, even for mollusks that typically maintain pH_{CF} below pH_{sw} under nonacidified conditions. Furthermore, 9 of the 10 species investigated increased the magnitude that pH_{CF} was elevated above pH_{sw} with decreasing pH_{sw}. Assuming that additional energy is required to in-crease this pH_{CF}-pH_{sw} differential, these results support prior assertions that biocalcification will be energetically more expensive for most, if not all, calcifying species under future, higher-pCO_2 conditions.

MATERIALS AND METHODS
Specimen culturing
Ten species of marine calcifiers—the blue crab, *Callinectes sapidus*; the gulf shrimp, *Penaeus plebejus*; the purple urchin, *Arbacia punctulata*; a coralline red alga *Neogoniolithon* sp.; the blue mussel, *Mytilus edulis*; a temperate coral, *Oculina arbuscula*; the pencil urchin, *Eucidaris tribuloides*; a hard clam, *Mercenaria mercenaria*; a serpulid worm, *Hydroides crucigera*; and the eastern oyster, *Crassostrea virginica*—were subsampled from the prior study (5). These species were previously shown to exhibit a wide range of calcification responses to CO_2-induced OA, including negative, threshold, neutral, parabolic, and positive. A detailed description of the culturing conditions is available in Ries *et al.* (5). In brief, specimens were cultured under four different pCO_2 conditions (409, 606, 903, and 2856 µatm) for 60 days in in seawater at constant temperature (25°C) and salinity (32 PSU). Calcium carbonate formed exclusively under experimental conditions by these 10 species was identified relative to a ^{137}Ba spike emplaced at the start of the experiment. The salinity, pH, and total alkalinity of the experimental treatments were monitored throughout the duration of the experiment. Calcification rates were estimated from the percent change in buoyant weight of the specimens between the beginning and end of the experiment.

Three specimens of each species from each of the four pCO_2 treatments (12 specimens total per species) were randomly selected for boron isotope analysis. However, only two specimens of the pencil urchin in the 606-µatm pCO_2 treatment, the hard clam in the 409-, 606-, and 903-µatm pCO_2 treatments, and the blue crab in the 409- and 606-µatm pCO_2 treatments were analyzed due to insufficient sample material. Calcium carbonate produced exclusively under the experimental conditions (identified relative to a Ba^{137} isotope marker emplaced in the skeleton at the start of the experiment) was obtained with a scalpel, gently pulverized in an agate mortar and pestle, and homogenized for boron isotopic analyses. The calcification responses of each species were defined with regression analyses and corresponding 95% confidence intervals. Of the 10 species investigated, only the blue mussel did not exhibit statistically significant trends in calcification rate as a function of seawater calcium carbonate saturation state (fig. S1).

MC-ICPMS measurements of boron
Boron isotopic compositions of the coralline red algae, pencil urchins, purple urchins, temperate corals, and serpulid worms were measured on a Thermo Finnigan Neptune MC-ICPMS (multicollector–inductively coupled plasma mass spectrometer) at Institut Français de Recherche pour l'Exploitation de la Mer (IFREMER), France, following the method from Sutton *et al.* (19).

Briefly, ca. 2 mg of dry sample was weighed and placed into an acid-cleaned microcentrifuge tube. The weighed samples were oxidized using a mixture of 200 µl of 1% NH_4OH and 1% H_2O_2 and placed in an ultrasonic bath for 10 min. This was followed by 1 min of centrifugation, after which the supernatant was removed. The oxidation step was then repeated, after which the samples were rinsed with 400 µl of UHQ (ultra-high-purity water sourced from a Millipore Direct-Q water purification system with a specific resistivity

of 18.2 megaohm·cm) in an sonic bath for 10 min, and then centrifuged for 1 min—after which the supernatant was removed and measured for pH. The rinsing process was repeated until pH of the supernatant reached ca. 7, indicating removal of NH_4OH. Samples were then washed with 20 μl of 0.001 M HNO_3 and rinsed with 400 μl of UHQ water as described above. Samples were then dissolved in a mixture of 300 μl of 0.05 M HNO_3 and 70 μl of 3 N HNO_3 for ca. 20 hours. Approximately 180 μl of 2% NH_4OH was added after the dissolution of the carbonate material to bring the pH back up to ca 7 to 8, which is required to successfully recover boron with the exchange resin used [Amberlite IRA 743; (27)].

Following the batch method described by Sutton *et al.* (19), Amberlite IRA 743 resin was used to extract boron from the sample matrices (19). Roughly 20 μl of Amberlite IRA 743 resin (crushed and sieved to a 100 to 200 mesh) was placed in a 500-μl acid-cleaned centrifuge tube and cleaned with 500 μl of 0.5 N HNO_3 to remove boron absorbed by the resin. Following the acid wash, the resin was rinsed three times with UHQ water (buffered to pH 7 with 2% NH_4OH) three times to elute unwanted cations and to condition the resin to pH 7. A cleaned and conditioned dissolved carbonate sample (see above for details) was then placed into a microcentrifuge tube containing clean resin. The vial was capped and shaken for 30 min to ensure that the sample solution contacted the resin. The mixture was then centrifuged for 1 min and decanted. The resin was rinsed with 200 μl of UHQ three times for 15 min to wash out the cations from the solution. Afterward, boron was recovered by adding 500 μl of 0.05 N HNO_3 to the vials and allowing 15 min for ion exchange. After 1 min of centrifugation, the supernatant was transferred to an acid-cleaned 2-ml vial and analyzed for boron concentration and isotope composition using a MC-ICPMS.

To reduce boron memory effects [see Sutton *et al.* (19) for details], we applied an in-line ammonia gas flush with 3.0-ml/min flow rate. To account for drift in mass discrimination during analysis, samples were bracketed by standards (NIST SRM951) of similar concentrations to the samples [ca. 65 parts per billion (ppb) of boron in 0.05 N HNO_3]. The mean values and reproducibilities of the international coral standard JCp-1 and a laboratory coral standard, NEP, are 25.15 ± 0.87‰ (2σ, *n* = 5) and 26.18 ± 1.04‰ (2σ, *n* = 5), respectively.

TE-NTIMS measurements of B
Boron isotopic compositions of the crabs, shrimp, oysters, and hard clams were measured on a Thermo Finnigan Triton multicollector thermal ionization mass spectrometry (TIMS) under negative ion mode at the Institute of Earth Sciences, Academia Sinica, Taiwan. The total evaporation NTIMS (TE-NTIMS) method was applied to overcome the low concentration of boron in the shells of the crustacea and mollusks and high organic content in the crustacea. Samples were prepared for TE-NTIMS analysis via microsublimation of the sample solution to remove organic matter (e.g., CNO^-) (28), which is known to interfere with boron analysis via negative thermal ionization mass spectrometry (NTIMS). This method was developed for and applied to measuring boron isotopes within a range of sample types, including seawater and bivalve shells (29, 30).

Cleaning, purification, and analysis of boron isotopes via TE-NTIMS followed the procedure from Liu *et al.* (30). In brief, sample powders were first cleaned with high-purity Milli-Q (MQ) water in an ultrasonic bath three times and then centrifuged, after which the supernatant was removed. Samples were then treated overnight with 10% H_2O_2 buffered with NaOH at room temperature to remove or-

ganic particles from the sample matrix. The samples were rinsed with MQ water, then with 0.001 N HNO_3, and then with MQ water again. After drying at 60°C, samples were weighed and dissolved in ca. 1.7 N HCl, yielding a boron concentration of approximately 750 ppb. Less than 50 μl of sample solution was loaded onto the cap of a conical-bottom vial in an inverted position and put into the high-throughput system described in Liu *et al.* (29). To further clean the samples and improve reproducibility of the boron analysis of the calcium carbonate samples, an extra 2 μl of 30% H_2O_2 was added to the purified solution and reacted for 2 hours. One microliter of the purified solution was then loaded onto outgassed Re filament for a single run using the total evaporation method. The mean value and reproducibility of the coral standard NEP before the replacement of the ion source was 24.54 ± 1.73‰ (2σ, *n* = 6). After replacement of the ion source, the mean values and reproducibility of the coral standards JCp-1 and NEP were 23.71 ± 1.64‰ (2σ, *n* = 15) and 25.56 ± 1.94‰ (2σ, *n* = 6), respectively.

Comparison of the accuracy and precision of the MC-ICPMS and TE-NTIMS methods for analyzing boron isotope composition
The mean values and reproducibility of carbonate standards JCp-1 and NEP measured on MC-ICPMS were 25.15 ± 0.87‰ (2σ, *n* = 5) and 26.18 ± 1.04‰ (2σ, *n* = 5), respectively. This results in an uncertainty in calculated pH_{CF} of 0.09 to 0.10 pH units. The mean values and reproducibility of NEP on TE-NTIMS (before and after the replacement of the ion source) was 24.54 ± 1.73‰ (2σ, *n* = 6) and 25.56 ± 1.94‰ (2σ, *n* = 6), respectively, resulting in an uncertainty in calculated pH_{CF} of ca. 0.18 pH units. The long-term mean value and reproducibility of JCp-1 measured on TE-NTIMS was 23.71 ± 1.64‰ (2σ, *n* = 15). Although the precision of the $δ^{11}B$ data obtained by MC-ICPMS was higher than that obtained by TE-NTIMS, the total sample required for TE-NTIMS analysis is about 1/20 of that required for MC-ICPMS, rendering TE-NTIMS the optimal method for analyzing the boron isotopic composition of calcium carbonate samples with low boron concentrations.

Calculations of pH and carbonate system parameters
Boron isotopic composition of the measured biogenic carbonates was converted to calcification site pH (pH_{CF}) with the following equation

$$pH_{CF} = pK_B - \log\left(\frac{δ^{11}B_{sw} - δ^{11}B_{CaCO3}}{α \times δ^{11}B_{CaCO3} - δ^{11}B_{sw} + 1000(α - 1)}\right)$$

where $δ^{11}B_{CaCO3}$ is $δ^{11}B$ of biogenic calcium carbonate, $pK_B = 8.6152$ at 25°C and 32 PSU (31), $δ^{11}B_{sw}$ ($δ^{11}B$ of total seawater boron) = 39.61‰ (32), and α = 1.0272 (21). The uncertainties and assumptions have been explored for a number of the investigated species in previous publications (16, 19) and are reviewed here in the Supplementary Materials.

The offset between pH_{sw} and pH_{CF} is defined as $ΔpH = pH_{CF} - pH_{sw}$. The analytical errors (2σ) of the boron isotopic analyses, derived from repeat analyses of samples, seawater, and standards, were 0.87‰ and 1.73‰ for the MC-ICPMS and TE-NTIMS methods, respectively. This analytical error was propagated through the pH_{CF} calculations via the Monte Carlo simulation. Propagated uncertainties were between 0.03 and 0.91 pH units.

Full seawater carbonate chemistry of each replicate experimental treatment was determined from the direct measurement of seawater

parameters, including pCO$_2$, temperature, salinity, total alkalinity, and pH, and has been previously reported (table S1) (*5*).

Statistical methods

All regression analyses were performed via least squares method, with linear and quadratic models used to investigate general trends in the data. The regression analysis and corresponding 95% confidence interval that minimized the root mean square error (RMSE) are shown in Fig. 1 and fig. S1 and described in tables S2 and S3. Note that regression models only represent general trends of the data and do not necessarily implicate specific physical or biological mechanism(s).

SUPPLEMENTARY MATERIALS

Supplementary material for this article is available at http://advances.sciencemag.org/cgi/content/full/6/5/eaax1314/DC1

Section S1. Species selection
Section S2. Consideration of the potential for non-pH effects on calcium carbonate δ^{11}B
Fig. S1. Calcification response patterns of the full sample collection and of the subset of samples used in this study.
Table S1. Seawater chemistry (pCO$_2$ in μatm, total alkalinity (TA) in umol/kg-SW, pH$_{sw}$), net calcification rate (% change/60 days), δ^{11}B (‰) of biogenic CaCO$_3$, calcification site pH (pH$_{CF}$), and ΔpH (pH$_{CF}$ − pH$_{sw}$).
Table S2. Linear and quadratic regression analysis of boron isotopic composition (δ^{11}B) of biogenic carbonates as a function of seawater pH via the least squares method.
Table S3. Linear and quadratic regression analysis of ΔpH as a function of seawater pH via the least squares method.
References (*33–41*)

REFERENCES AND NOTES

1. S. C. Doney, V. J. Fabry, R. A. Feely, J. A. Kleypas, Ocean acidification: The other CO$_2$ problem. *Ann. Rev. Mar. Sci.* **1**, 169–192 (2009).
2. IPCC, *Climate change 2014: synthesis report. Contribution of Working Groups I, II and III to the fifth assessment report of the Intergovernmental Panel on Climate Change*, Core Writing Team, R.K, Pachauri, L.A. Meyer, Eds. (IPCC, 2014), pp. 151.
3. J. C. Orr, V. J. Fabry, O. Aumont, L. Bopp, S. C. Doney, R. A. Feely, A. Gnanadesikan, N. Gruber, A. Ishida, F. Joos, R. M. Key, K. Lindsay, E. Maier-Reimer, R. Matear, P. Monfray, A. Mouchet, R. G. Najjar, G.-K. Plattner, K. B. Rodgers, C. L. Sabine, J. L. Sarmiento, R. Schlitzer, R. D. Slater, I. J. Totterdell, M.-F. Weirig, Y. Yamanaka, A. Yool, Anthropogenic ocean acidification over the twenty-first century and its impact on calcifying organisms. *Nature* **437**, 681–686 (2005).
4. G. E. Hofmann, J. P. Barry, P. J. Edmunds, R. D. Gates, D. A. Hutchins, T. Klinger, M. A. Sewell, The effect of ocean acidification on calcifying organisms in marine ecosystems: An organism-to-ecosystem perspective. *Annu. Rev. Ecol. Evol. Syst.* **41**, 127–147 (2010).
5. J. B. Ries, A. L. Cohen, D. C. McCorkle, Marine calcifiers exhibit mixed responses to CO$_2$-induced ocean acidification. *Geology* **37**, 1131–1134 (2009).
6. K. J. Kroeker, R. L. Kordas, R. Crim, I. E. Hendriks, L. Ramajo, G. S. Singh, C. M. Duarte, J.-P. Gattuso, Impacts of ocean acidification on marine organisms: Quantifying sensitivities and interaction with warming. *Glob. Chang. Biol.* **19**, 1884–1896 (2013).
7. J. Meyer, U. Riebesell, Reviews and syntheses: Responses of coccolithophores to ocean acidification: a meta-analysis. *Biogeosciences* **12**, 1671–1682 (2015).
8. M. N. Müller, T. W. Trull, G. M. Hallegraeff, Differing responses of three Southern Ocean Emiliania huxleyi ecotypes to changing seawater carbonate chemistry. *Mar. Ecol. Prog. Ser.* **531**, 81–90 (2015).
9. J. B. Ries, A physicochemical framework for interpreting the biological calcification response to CO$_2$-induced ocean acidification. *Geochim. Cosmochim. Acta* **75**, 4053–4064 (2011).
10. L. Addadi, S. Raz, S. Weiner, Taking advantage of disorder: Amorphous calcium carbonate and its roles in biomineralization. *Adv. Mater.* **15**, 959–970 (2003).
11. N. Vidavsky, S. Addadi, A. Schertel, D. Ben-Ezra, M. Shpigel, L. Addadi, S. Weiner, Calcium transport into the cells of the sea urchin larva in relation to spicule formation. *Proc. Natl. Acad. Sci. U.S.A.* **113**, 12637–12642 (2016).
12. T. Mass, A. J. Giuffre, C.-Y. Sun, C. A. Stifler, M. J. Frazier, M. Neder, N. Tamura, C. V. Stan, M. A. Marcus, P. U. P. A. Gilbert, Amorphous calcium carbonate particles form coral skeletons. *Proc. Natl. Acad. Sci. U.S.A.* **114**, E7670–E7678 (2017).
13. S. Von Euw, Q. Zhang, V. Manichev, N. Murali, J. Gross, L. C. Feldman, T. Gustafsson, C. Flach, R. Mendelsohn, P. G. Falkowski, Biological control of aragonite formation in stony corals. *Science* **356**, 933–938 (2017).
14. C. E. Cornwall, S. Comeau, T. M. DeCarlo, B. Moore, Q. D'Alexis, M. T. McCulloch, Resistance of corals and coralline algae to ocean acidification: Physiological control of calcification under natural pH variability. *Proc. Biol. Sci.* **285**, 20181168 (2018).
15. H. K. Donald, J. B. Ries, J. A. Stewart, S. E. Fowell, G. L. Foster, Boron isotope sensitivity to seawater pH change in a species of *Neogoniolithon* coralline red alga. *Geochim. Cosmochim. Acta* **217**, 240–253 (2017).
16. Y.-W. Liu, R. A. Eagle, S. M. Aciego, R. E. Gilmore, J. B. Ries, A coastal coccolithophore maintains pH homeostasis and switches carbon sources in response to ocean acidification. *Nat. Commun.* **9**, 2857 (2018).
17. M. T. McCulloch, J. P. D'Olivo, J. Falter, M. Georgiou, P. Holcomb, P. Montagna, J. A. Trotter, Boron isotopic systematics in scleractinian corals and the role of pH up-regulation, in *Boron Isotopes: The Fifth Element*, H. Marschall, G. Foster, Eds. (Springer International Publishing, Cham, 2018), pp. 145–162.
18. D. E. Penman, B. Hönisch, E. T. Rasbury, N. G. Hemming, H. J. Spero, Boron, carbon, and oxygen isotopic composition of brachiopod shells: Intra-shell variability, controls, and potential as a paleo-pH recorder. *Chem. Geol.* **340**, 32–39 (2012).
19. J. N. Sutton, Y.-W. Liu, J. B. Ries, M. Guillermic, E. Ponzevera, R. A. Eagle, δ^{11}B as monitor of calcification site pH in divergent marine calcifying organisms. *Biogeosciences* **15**, 1447–1467 (2018).
20. J. W. B. Rae, Boron isotopes in foraminifera: Systematics, biomineralisation, and CO2 reconstruction, in *Boron Isotopes: The Fifth Element*, H. Marschall, G. Foster, Eds. (Springer International Publishing, Cham, 2018), pp. 107–143.
21. K. Klochko, A. J. Kaufman, W. Yao, R. H. Byrne, J. A. Tossell, Experimental measurement of boron isotope fractionation in seawater. *Earth Planet. Sci. Lett.* **248**, 276–285 (2006).
22. F. A. Al-Horani, S. M. Al-Moghrabi, D. de Beer, The mechanism of calcification and its relation to photosynthesis and respiration in the scleractinian coral Galaxea fascicularis. *Mar. Biol.* **142**, 419–426 (2003).
23. A. A. Venn, E. Tambutté, M. Holcomb, J. Laurent, D. Allemand, S. Tambutté, Impact of seawater acidification on pH at the tissue–skeleton interface and calcification in reef corals. *Proc. Natl. Acad. Sci. U.S.A.* **110**, 1634–1639 (2013).
24. M. A. Crenshaw, The inorganic composition of molluscan extrapallial fluid. *Biol. Bull.* **143**, 506–512 (1972).
25. J. B. Ries, M. N. Ghazaleh, B. Connolly, I. Westfield, K. D. Castillo, Impacts of seawater saturation state (ΩA = 0.4–4.6) and temperature (10, 25 °C) on the dissolution kinetics of whole-shell biogenic carbonates. *Geochim. Cosmochim. Acta* **192**, 318–337 (2016).
26. J. A. Short, O. Pedersen, G. A. Kendrick, Turf algal epiphytes metabolically induce local pH increase, with implications for underlying coralline algae under ocean acidification. *Estuar. Coast. Shelf Sci.* **164**, 463–470 (2015).
27. E. Kiss, Ion-exchange separation and spectrophotometric determination of boron in geological materials. *Anal. Chim. Acta* **211**, 243–256 (1988).
28. N. G. Hemming, G. N. Hanson, A procedure for the isotopic analysis of boron by negative thermal ionization mass spectrometry. *Chem. Geol.* **114**, 147–156 (1994).
29. Y.-W. Liu, S. M. Aciego, A. D. Wanamaker Jr., B. K. Sell, A high-throughput system for boron microsublimation and isotope analysis by total evaporation thermal ionization mass spectrometry. *Rapid Commun. Mass Spectrom.* **27**, 1705–1714 (2013).
30. Y.-W. Liu, S. M. Aciego, A. D. Wanamaker Jr., Environmental controls on the boron and strontium isotopic composition of aragonite shell material of cultured *Arctica islandica*. *Biogeosciences* **12**, 3351–3368 (2015).
31. A. G. Dickson, Thermodynamics of the dissociation of boric acid in synthetic seawater from 273.15 to 318.15 K. *Deep Sea Res. Part A* **37**, 755–766 (1990).
32. G. L. Foster, P. A. E. Pogge, von Strandmann, J. W. B. Rae, Boron and magnesium isotopic composition of seawater. *Geochem. Geophys. Geosyst.* **11**, Q08015 (2010).
33. J. B. Ries, Skeletal mineralogy in a high-CO$_2$ world. *J. Exp. Mar. Bio. Ecol.* **403**, 54–64 (2011).
34. E. Balan, F. Pietrucci, C. Gervais, M. Blanchard, J. Schott, J. Gaillardet, First-principles study of boron speciation in calcite and aragonite. *Geochim. Cosmochim. Acta* **193**, 119–131 (2016).
35. J. R. Farmer, O. Branson, J. Uchikawa, D. E. Penman, B. Hönisch, R. E. Zeebe, Boric acid and borate incorporation in inorganic calcite inferred from B/Ca, boron isotopes and surface kinetic modeling. *Geochim. Cosmochim. Acta* **244**, 229–247 (2019).
36. V. Mavromatis, V. Montouillout, J. Noireaux, J. Gaillardet, J. Schott, Characterization of boron incorporation and speciation in calcite and aragonite from co-precipitation experiments under controlled pH, temperature and precipitation rate. *Geochim. Cosmochim. Acta* **150**, 299–313 (2015).
37. J. Noireaux, V. Mavromatis, J. Gaillardet, J. Schott, V. Montouillout, P. Louvat, C. Rollion-Bard, D. R. Neuville, Crystallographic control on the boron isotope paleo-pH proxy. *Earth Planet. Sci. Lett.* **430**, 398–407 (2015).
38. G. D. Saldi, J. Noireaux, P. Louvat, L. Faure, E. Balan, J. Schott, J. Gaillardet, Boron isotopic fractionation during adsorption by calcite – implication for the seawater pH proxy. *Geochim. Cosmochim. Acta* **240**, 255–273 (2018).

39. M. Stumpp, M. Y. Hu, F. Melzner, M. A. Gutowska, N. Dorey, N. Himmerkus, W. C. Holtmann, S. T. Dupont, M. C. Thorndyke, M. Bleich, Acidified seawater impacts sea urchin larvae pH regulatory systems relevant for calcification. *Proc. Natl. Acad. Sci. U.S.A.* **109**, 18192–18197 (2012).

40. M. Cusack, N. A. Kamenos, C. Rollion-Bard, G. Tricot, Red coralline algae assessed as marine pH proxies using ^{11}B MAS NMR. *Sci. Rep.* **5**, 8175 (2015).

41. L. C. Hofmann, K. Schoenrock, D. de Beer, Arctic coralline algae elevate surface pH and carbonate in the dark. *Front. Plant Sci.* **9**, 1416 (2018).

Citation: Y.-W. Liu, J. N. Sutton, J. B. Ries, R. A. Eagle, Regulation of calcification site pH is a polyphyletic but not always governing response to ocean acidification. *Sci. Adv.* **6**, eaax1314 (2020).

Science Advances

Regulation of calcification site pH is a polyphyletic but not always governing response to ocean acidification

Yi-Wei Liu, Jill N. Sutton, Justin B. Ries and Robert A. Eagle

ARTICLE TOOLS	http://advances.sciencemag.org/content/6/5/eaax1314
SUPPLEMENTARY MATERIALS	http://advances.sciencemag.org/content/suppl/2020/01/27/6.5.eaax1314.DC1
REFERENCES	This article cites 38 articles, 6 of which you can access for free http://advances.sciencemag.org/content/6/5/eaax1314#BIBL
PERMISSIONS	http://www.sciencemag.org/help/reprints-and-permissions